Facile method to reduce surface defects and trap densities in perovskite photovoltaics

Guifang Han[†], Teck Ming Koh[†], Swee Sien Lim[‡,§], Teck Wee Goh[‡], Xintong Guo[‖,§], Shin Woei Leow[‖†], Raihana Begum[†], Tze Chien Sum[‡], Nripan Mathews[†‖], Subodh Mhaisalkar[†‖*]*

[†] Energy Research Institute @NTU (ERI@N), Nanyang Technological University, Research Techno Plaza, X-Frontier Block, Level 5, 50 Nanyang Drive, 637553, Singapore

[‡]Division of Physics and Applied Physics, School of Physical and Mathematical Sciences, Nanyang Technological University, 21 Nanyang Link, 637371, Singapore

[§]Interdisciplinary Graduate School, Nanyang Avenue, 639798, Singapore

[‖]School of Materials Science and Engineering, Nanyang Technological University, Nanyang Avenue, 639798, Singapore

*(N.M.): E-mail: Nripan@ntu.edu.sg., *(S.P.M.): E-mail: Subodh@ntu.edu.sg

KEYWORDS: Perovskite, trap density, photovoltaics, Methylammonium bromide treatment, surface defect, passivation, grain growth

ABSTRACT:

Owing to improvements in film morphology, crystallization process optimization and compositional design, the power conversion efficiency of perovskite solar cells have increased from 3.8% to 22.1% in a period of five years. Nearly defect-free crystalline films and slow recombination rates enable polycrystalline perovskite to boast efficiencies comparable with multi-crystalline silicon solar cells. However, volatile low melting point components and anti-solvent treatments essential for the processing of dense and smooth films, often lead to surface defects hampering charge extraction. In this study, we investigate methylammonium bromide (MABr) surface treatments on perovskite films, to compensate for the loss of volatile cation during the annealing process, for surface defect passivation, grain growth and a bromide-rich top layer. This facile method did not change the phase or bandgap of perovskite films, yet resulted in a significant increase in the open circuit voltages of devices. The devices with 10 mM MABr treatment show 2% improvement in absolute power conversion efficiency over the control sample.

▪ INTRODUCTION

Benefiting from a high absorption coefficient, long carrier life time and diffusion length,[1-3] perovskite based solar cells have attained a power conversion efficiency (PCE) greater than 22% within five years.[4] The facile composition tunability and solution processability of perovskite has opened up a new era of low-cost thin film solar cells. The quality of polycrystalline perovskite films can be optimized through compositional design and process control. Among hybrid perovskites, formamidinium lead iodide ($FAPbI_3$) exhibits a relatively lower bandgap compared to methylammonium lead iodide ($MAPbI_3$), allowing for the absorption of light with longer

wavelengths.[5] However, $FAPbI_3$ tends to form/degrade to a non-photoactive δ-phase which drastically reduces device performance.[5] Adding methylammonium lead bromide ($MAPbBr_3$) into $FAPbI_3$ not only retards the formation of the δ-phase in $FAPbI_3$, it also tunes the bandgap closer to the optimum range for photovoltaics.[6] Further addition of cesium (Cs) into this mixture, forming the so-called triple-cation perovskite, resulted in faster crystallization during spin coating, improving the quality and reproducibility of perovskite films.[7] Recently, a quadruple cation perovskite solar cell was reported with Rubidium iodide (RbI) added into the triple-cation system, boosting solar cell efficiency to more than 20%. [8] New perovskite deposition techniques, such as anti-solvent [9-10] and vacuum flash [11] methods, enable formation of high quality films with large mono-grains perpendicular to the substrate. This facilitates good charge transport and collection leading to additional efficiency gains. These advancements have undoubtedly led to the rise in polycrystalline perovskite device performance that rival multi-crystal silicon solar cells.

Shallow defect energy levels, and slow electron-hole recombination process,[2] makes perovskites more tolerant to defect or traps. However, the effects of grain boundaries are still evident. Single crystal perovskite shows extremely low trap density (5.8×10^9 cm^{-3} and 3.3×10^{10} $cm^{-3}$for $MAPbBr_3$ and $MAPbI_3$ respectively), and high mobility (115 cm^2 V^{-1} s^{-1} for electron and hole in $MAPbBr_3$ single crystal).[12] This is several orders better than that of polycrystalline perovskite films, with a trap density in the order of 10^{16} cm^{-3}, [13-14] and mobility of 1~5 $cm^2V^{-1}s^{-1}$ for holes and 5~10 $cm^2V^{-1}s^{-1}$ for electrons.[15] Solvent assisted annealing, [16] hot casting [17] and selective Ostwald ripening [18] strategies have empirically confirmed that perovskites with larger grain size exhibit lower trap densities and better solar cell device performances. In addition, we recently investigated the recombination mechanism in single crystal and also polycrystalline perovskite solar cells with

different absorber thicknesses, and the results point to surface recombination as the dominant mechanism. [19-20]

Loss of iodine at the surface of perovskites creates vacancy sites, resulting in a net positive charge residing on the Pb atom. Based on this, Snaith and coworkers [14] utilised Lewis bases such as thiophene and pyridine, which donate electrons and passivate the defects resulting in reduced non-radiative recombination. Heben et al. showed that the vaporization of MAI at high temperatures necessitates an excess of MAI to form a stoichiometric $MAPbI_3$ film.[21] Although, $FAPbI_3$ is known to exhibit better thermal stability than $MAPbI_3$,[22] our experimental results with stoichiometric precursor ratios (molar ratio of FAI : PbI_2 = 1:1) suggest that FAI is still lost during annealing, as evidenced by a peak corresponding to PbI_2 in the XRD (**Figure S1)**. Increasing annealing time to 30 min causes the PbI_2 peak to become even more pronounced. From these findings, we can infer that during the annealing process, low boiling point components vaporize from the perovskite film forming a multitude of defect states, especially at the film's surface. Lim et al. also showed that anti-solvent treatment increases trap densities due to the formation of MA vacancies in the perovskite films. [23]

Figure 1 (atoms highlighted in yellow) illustrates the loss of both halogen and organic cation forming vacancy defects. Herein, we introduce a facile method to passivate the defects and compensate for the loss of MABr/FAI in the triple-cation perovskite crystal structure. On the surface of triple-cation perovskite films, a very thin layer of MABr is spin-coated. The advantage of this simple, yet critical step is that during post-anneal, MA^+ and Br^- ions can diffuse into the vacancies created by the loss of organic cations and I^-, thus passivating the defects (arrows in **Figure 1)**. In addition, the relatively low melting point MABr can help to increase the grain size of films through Ostwald ripening phenomenon during annealing, which lowers the grain boundary

areas and further decreases the trap density of perovskite films. The decrease in trap density is expected to improve device performances, especially the open-circuit voltage (V_{oc}). [18]

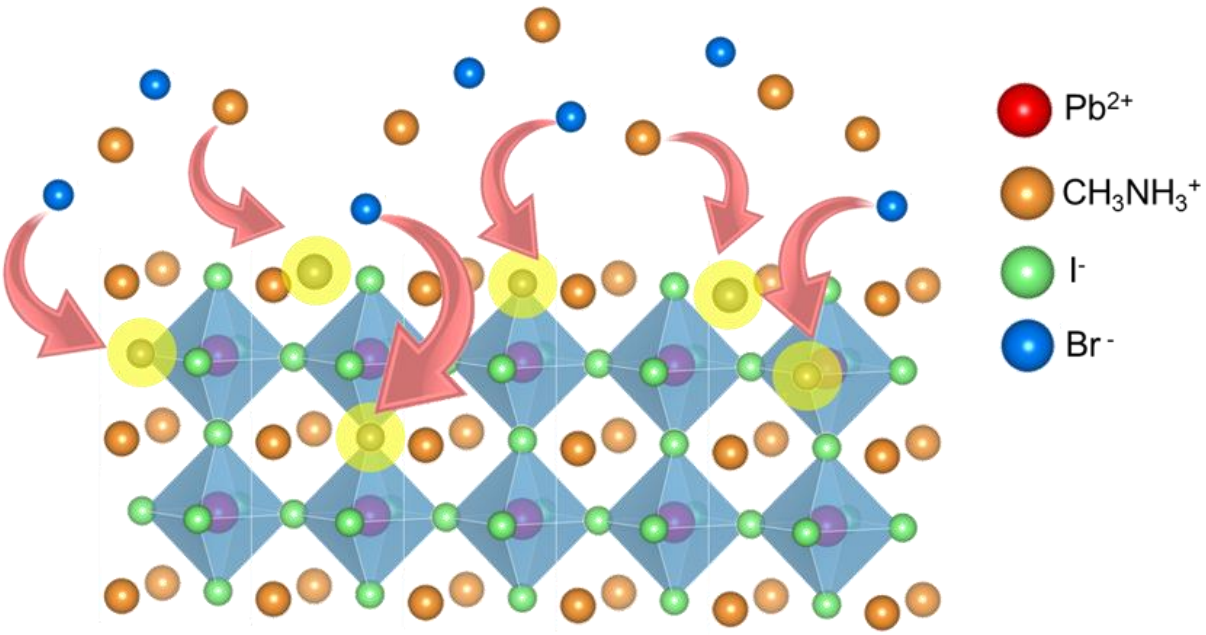

Figure 1 Schematic concept of defects and defects filling, where MA+ (orange) and Br- (blue)ions fill vacancies as indicated by the arrows

▪ RESULTS AND DISCUSSIONS

The fabrication procedure is schematically represented in **Figure 2a**. Triple-cation perovskite $(FA_{0.83}MA_{0.17})_{0.95}Cs_{0.05}Pb(I_{0.83}Br_{0.17})_3$ with 10% excess Pb, is formed via the anti-solvent method and resulting films were annealed at 100°C for 60 mins using previously published procedures.[7] Next, MABr in isopropyl alcohol (IPA) with different concentrations were dropped onto the perovskite films, spun and heated at 70°C for 5min. Interestingly, V_{oc} of fabricated devices showed a continuous increase from 0.9 V to 1.05 V with increasing concentration of MABr solution

(**Figure 2b**). The maximum value of *J*sc obtained is around 21mA/cm^2 when treated with 10 mM MABr (**Figure 2c**). The fill factor didn't change so much, except at higher concentrations (25 mM MABr) (**Figure 2d**). The power conversion efficiency reached a maximum average value of 15.38% when treated with 10 mM MABr compared to 13.37% for the control devices (**Figure 2e**).

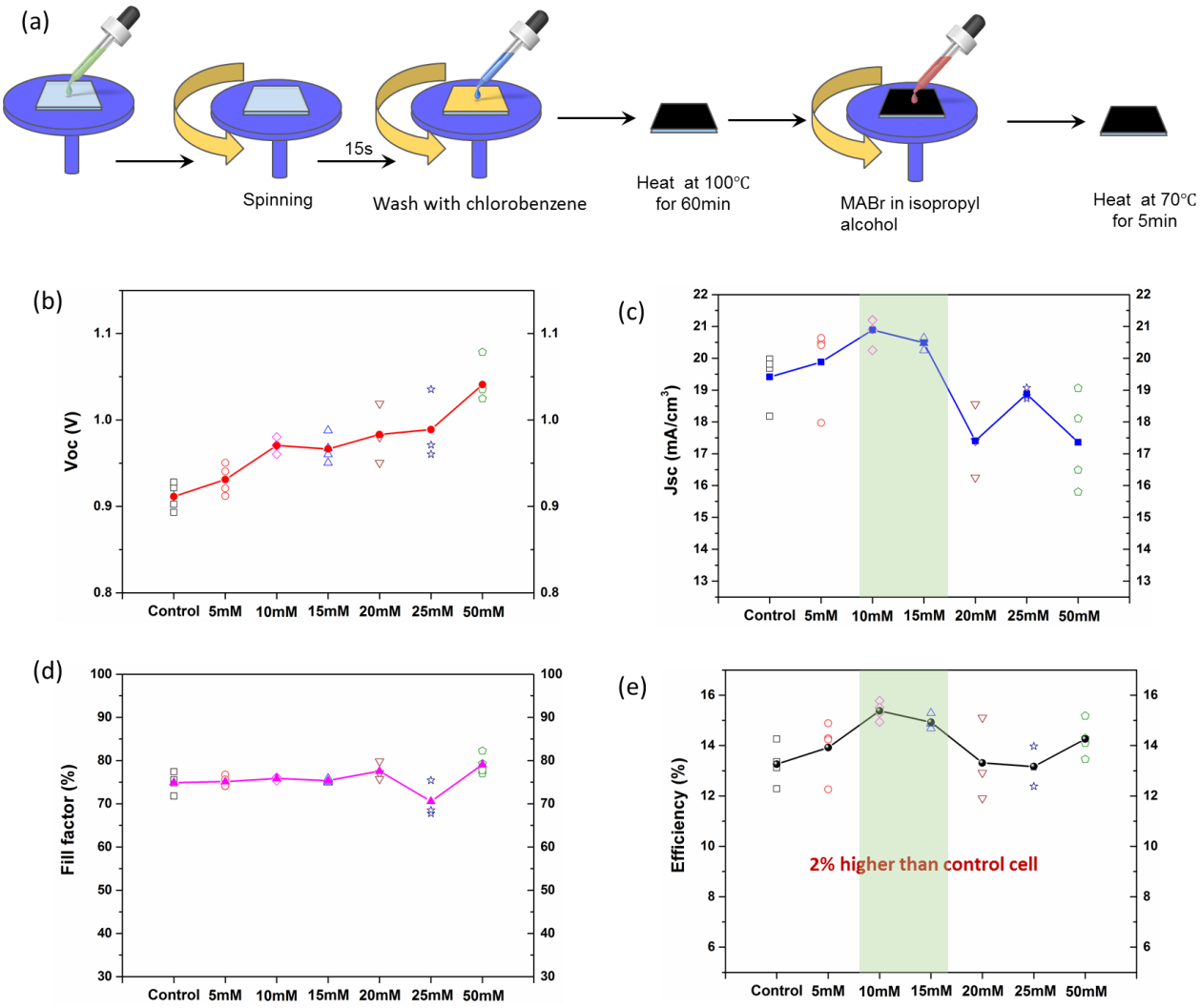

Figure 2 (a) Schematic figure of fabrication procedure, and variation of(b)open-circuit voltages (*V*oc), (c) short-circuit current density (*J*sc), (d) fill factor and (e) efficiencies of perovskite solar cell devices treated with different concentrations of MABr

To further investigate the reason behind this improvement of device performance, different characterization methods were applied. **Figure 3a** shows the surface and cross-section microstructure of the control and MABr treated perovskite films. As can be seen, before MABr treatment, the perovskite grain size is relatively uniform in the range of 50~100nm. Upon 10 mM MABr treatment, several larger grains appeared. With further increase of MABr concentration, the grain size increased significantly and an average grain size of around 600 nm is observed for the 50 mM MABr treated sample. This is corroborated by the cross-section view where there is a merging of grains vertically and horizontally up until 20 mM of MABr. Unexpectedly, the opposite occurs at 50mM concentration, where a separation of layers appears to have occurred. The grain boundaries of 50 mM treated films are more evident compared to lower MABr concentration samples. The annealing temperature of 70^{o}C used in this study is the same as that for annealing $MAPbBr_3$ films. We hypothesize that with high concentrations, enough MABr diffuses into the perovskite film that Br-rich grains begin to form which separate out from the bulk. However, from the X-ray diffraction analysis, no apparent difference in the phase was observed. Interestingly, the PbI_2 peak, which appeared in the un-treated sample, is diminished with increasing MABr concentration (**Figure 3b)**.

To check if the increase in Voc is due to an enlarged bandgap with the addition of bromide or a suppression of defects and larger grain sizes, optical absorption measurements were performed (**Figure 3c**). Extracted bandgaps show no change with only a slight difference with 50 mM MABr treated perovskite films. However, the increment is only from 1.62eV to 1.63eV, which cannot explain the *Voc* improvement with a value as high as 0.15V. In order to gauge the quality of the thin films, photoluminescence measurements were performed. Compared to the control sample, the Photoluminescence (PL) intensity is highest for 10 mM MABr treatment (**Figure 3d)**. The

increase of PL intensity indicates that MABr treatment resulted in reducing non-radiative trap states in the film.

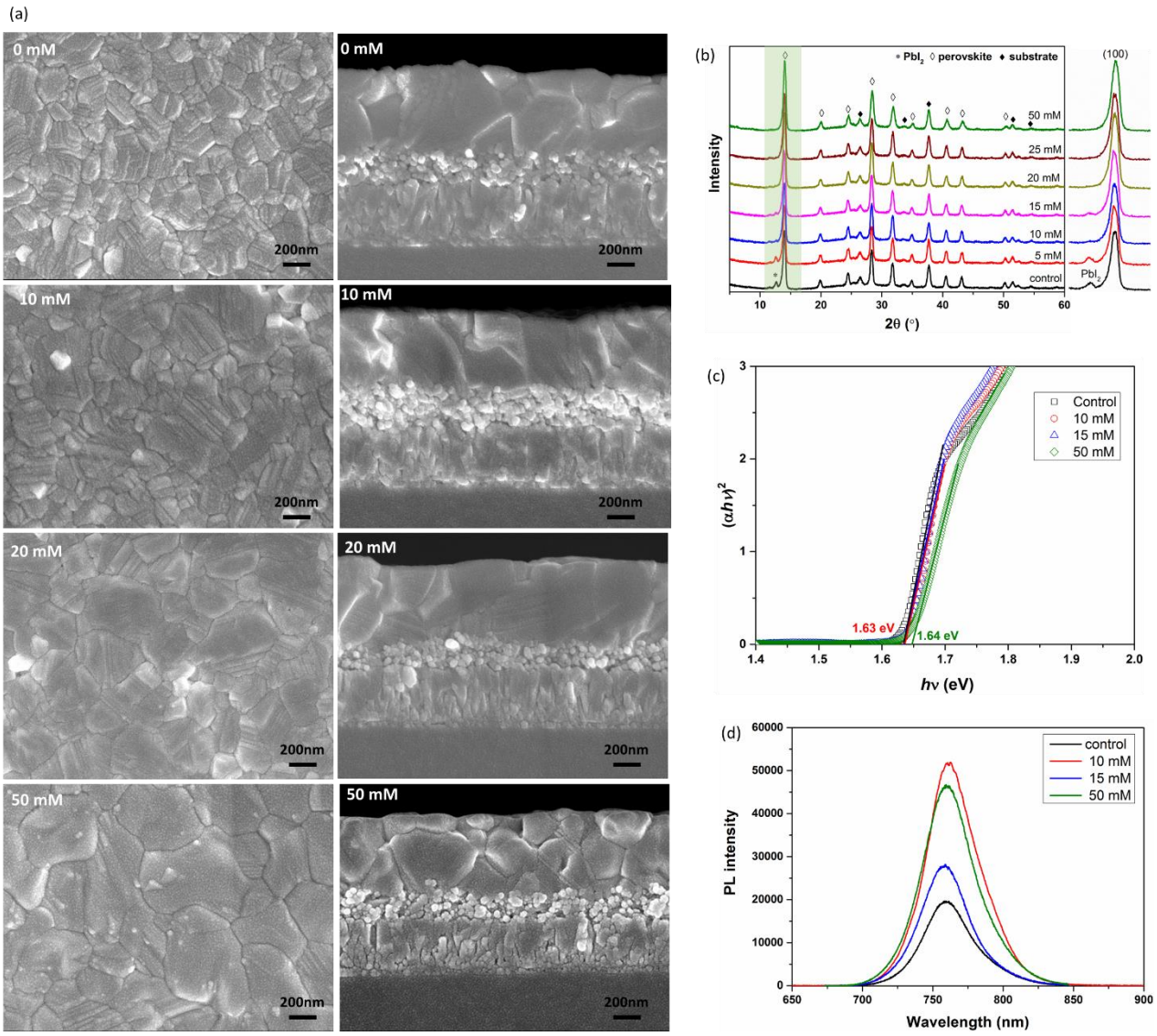

Figure 3(a) surface and cross-section microstructure, (b) XRD patterns, (c) Tauc plots and (d) photoluminescence of perovskite films treated with different concentration of MABr solution

X-ray photoelectron spectroscopy (XPS) was used to investigate the surface composition of the perovskite films upon MABr treatment (**Table 1)**. The detailed spectrum is shown in **Figure S2**.

For the un-treated films, the lead content (20.7%) is lower than the precursor (22%). The content of A-site cation is apparently less than the precursor, indicating cation deficiency. The binding energy of nitrogen in MA (CH_3NH_3) and FA ($HC(NH_2)_2$) is 402.79 eV and 401.21 eV, respectively. Based on this, the percentage of MA, FA and Cs cations can be determined, as listed in Table 1. On the surface of the control sample, only FA was detected without any trace of MA and Cs, which supports the hypothesis that the MA cation evaporated during annealing. When carefully compared, the Br content on the film surface was found to be much lower than that in the precursor, implying that Br is also deficient after annealing. This confirms our hypothesis. When 10 mM MABr solution was used to treat the surface of perovskite film, the cation content increases. MA appeared after this surface treatment. The content of I and Br is 81.42% and 18.58% respectively, which is comparable with the composition of I: 83% and Br: 17% in the triple cation solution precursor. When the concentration of MABr solution is further increased to 15mM and 50mM, the cation becomes sufficient and Pb tends to be deficient. Both the MA and Br content measured are much higher than the triple cation precursor. This might be because the MABr amount is now much higher than the optimal value required to compensate for losses during annealing as discussed earlier. Surface XPS results indicate that 10 mM MABr should be enough to passivate surface defects formed during the fabrication process. The highest efficiency obtained was with 10 mM MABr treated devices. The reduced short circuit current density of treated perovskite devices indicated that charge transport and collection are not efficient when the MABr concentration is higher than 15 mM (**Figure 2c**). This might be because the valance band maximum of 50 mM treated perovskite films is too low and might form a barrier that hinders hole transfer to spiro-o-MeTAD. The valence band maximum (VBM) position of the mixed cation system which we used here is similar to pure $MAPbI_3$ (VBM: -5.43 eV),[24] where the holes

generated could be effectively collected by the spiro layer (HOMO: -5.22 eV). The VBM of bromide systems are much lower than our mixed system ($MAPbBr_3$ of -5.58 eV and $FAPbBr_3$ of -5.6 eV).[25-26] We hypothesise that the Br-rich layer on the perovskite surface with higher MABr concentration, might move the VBM position downward acting as a barrier for holes thus inducing lower J_{sc} values.

Table 1 Surface composition of perovskite film treated with different concentration of MABr solution analyzed by XPS

MABr treatment	Cation A content (%)	Metal cation B content (%)	Halogen X content (%)
Precursor composition	20 (FA: 78.85%, MA: 16.15%, Cs: 5%)	22	60 (I: 83%, Br: 17%)
Control	13.69 (FA: 100%)	20.70	65.61 (I: 88.68%, Br: 11.32%)
10 mM	18.82 (FA: 70.46%, MA: 26.46%, Cs: 3.09%)	19.03	62.15 (I: 81.42%, Br: 18.58%)
15 mM	22.31 (FA: 72.00%, MA: 24.08%, Cs: 3.92%)	18.40	59.29 (I: 74.57%, Br: 25.43%)
50 mM	25.12 (FA: 60.94%, MA: 35.21%, Cs: 3.85%)	17.09	57.79 (I: 70.79%, Br: 29.21%)

To further investigate whether this treatment is only a surface effect, we conducted trap state density measurement. Power dependent steady-state PL in the low fluence regime (where there is negligible Auger recombination) is performed to estimate the trap densities using a model developed in an earlier work.[27] Briefly, the model assumes an infinite number of trapping pathways, each with their distinct trapping rates and trap densities. Pulses with wavelength of 600 nm were used to uniformly excite the bulk of the film. The variation of carrier density along with PL intensity is shown in **Figure 4**. For the control sample, the trap density is $3.2\pm0.2\times10^{17}$ cm^{-3}. It decreased to $1.37\pm0.09\times10^{17}$ cm^{-3} and $1.8\pm0.1\times10^{17}$ cm^{-3} for 10 mM and 15 mM MABr

treated samples, respectively. The trap density of the film further decreased to $0.55 \pm 0.08 \times 10^{17}$ cm^{-3} with 50 mM MABr treatment. As discussed above, the film microstructure of 50 mM MABr treated sample has more grain boundaries than others but shows the lowest trap density. This appears to be contradictory, since normally grain boundary in semiconductors acts as recombination centers. Besides the reported benign grain boundary in perovskite [28-29], our previous works on both single crystal [19] and polycrystalline thin films of perovskite [20] have showed that, surface recombination is the dominant process in perovskite materials. We suppose that in this case the grain boundary defects play a minor role so while defects due to grain boundaries might have increased, this increase is minor compared to the big reduction due to surface recombination reductions. In the surface composition study by XPS, 10 mM MABr seems to be enough to passivate the surface defects. However, the lowest trap density achieved is with 50 mM MABr treated film. With higher concentrations, the MABr might diffuse into the film, passivating bulk defects during annealing. The trap density measured during PL is a superposition of surface and bulk defects, and thus trap density is lowest with 50mM MABr treatment. The decreasing of trap density with MABr treatment clearly suggested that although our approach is largely a surface treatment, it also has an effect on the bulk. Reduced trap density improves the performance of devices, as seen in the 10 mM MABr treated samples, where it has low trap density and highest efficiencies.

However, if we carefully compare the value of trap density, one could find that the difference between trap density of the control ($3.2 \pm 0.2 \times 10^{-17}$ cm^{-3}) and 50 mM treated ($0.55 \pm 0.08 \times 10^{-17}$ cm^{-3}) samples is around 2.65×10^{-17} cm^{-3}, which include both shallow and deep traps. Normally shallow defects have less effect on the attainable *Voc*. W. Yang et al [30] calculated the theoretical relationship between density of deep trap states and the value of *Voc*, and found that the increase

of *Voc* is less than 0.1 V when the trap density is reduced from 5×10^{-17} cm^{-3} to 5×10^{-16} cm^{-3}. If we consider that the trap densities which we measured are all from deep trap states, the theoretical maximum improvement of *Voc* should be less than 0.06 V with the 50 mM MABr treatment. However, the average value of *Voc* increases from 0.91 V in the control samples to 1.04 V with 50 mM MABr treatment. The difference of 0.13 V is twice the predicated theoretical value and therefore the decrease of trap density cannot solely explain the improvement of *Voc* in our study. Reports have suggested that the *Voc* is dependent on the difference of energy levels between electron and hole selection layers,[31] while other reports indicate that the *Voc* is more likely decided by the perovskite materials itself. [32] As the electron and hole selection layers are identical in our studies, the first case is not relevant. As discussed previously, the surface of perovskite films might form a bromide rich phase during this treatment and the bromide perovskites have wider bandgaps and deeper VBM levels, which might help the increment of *Voc*. However, with too much MABr, the bromide rich phase might form a barrier for hole collection by spiro and decrease the current density, which coincides with our results. Therefore, the best overall performance obtained is with 10 mM MABr treated devices. However, further experimental investigation and proper physical models to explain the working mechanism of perovskite solar cells are still needed.

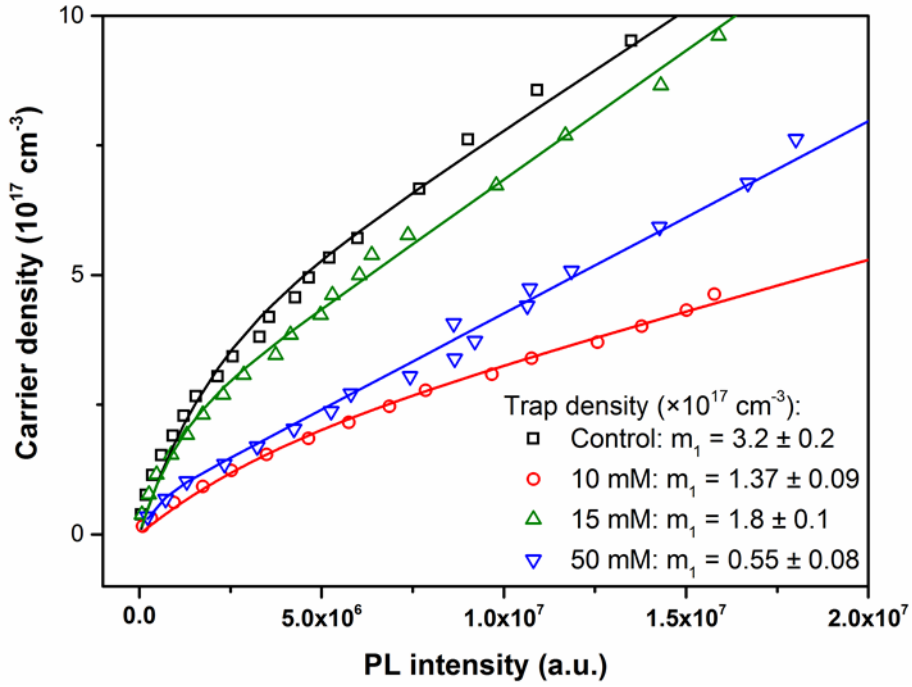

Figure 4 trap density measurements of perovskite films treated with different concentrations of MABr

▪ CONCLUSIONS

In summary, MABr is used to compensate for the volatile low boiling point components inside perovskite films during the annealing process, which also passivates the surface defects. The effect of different concentrations of MABr solution on device performance was investigated. The results showed that the grains first merged together and finally separated into two layers of grains with increasing MABr concentration. There was no apparent change in the crystal phase and bandgap (as estimated from absorption spectrum), however PL intensity increased with MABr treatment and reached a maximum when 10 mM of MABr was used. The open circuit voltage also increased with the increasing MABr concentration and average power conversion efficiencies improved from 13.37% to 15.38% with 10 mM MABr treatment, which originates from lower trap density and a thin bromide rich layer on top of perovskite films with MABr treatment. This study provides

a facile way to lower the trap density to improve the performance of perovskite materials for photovoltaic applications.

▪ ACKNOWLEDGMENTS

The authors acknowledge funding from the National Research Foundation, Prime Minister's Office, Singapore under its Competitive Research Program (CRP Award No. NRF-CRP14-2014-03) and through the Singapore–Berkeley Research Initiative for Sustainable Energy (SinBeRISE) CREATE Program; Nanyang Technological University start-up grants (M4080514 and M4081293); the Ministry of Education Academic Research Fund Tier 1 grants (RG184/14, RG166/16 and RG101/15), and Tier 2 grants (MOE2016-T2-1-100, MOE2014-T2-1-044 and MOE2015-T2-2-015).

▪ REFERENCES

(1) Sum, T. C.; Mathews, N. Advancements in Perovskite Solar Cells: Photophysics behind the Photovoltaics. *Energy Environ. Sci.* **2014,** *7*, 2518-2534.
(2) Leijtens, T.; Eperon, G. E.; Barker, A. J.; Grancini, G.; Zhang, W.; Ball, J. M.; Kandada, A. R. S.; Snaith, H. J.; Petrozza, A. Carrier Trapping and Recombination: the Role of Defect Physics in Enhancing the Open Circuit Voltage of Metal Halide Perovskite Solar Cells. *Energy Environ. Sci.* **2016,** *9*, 3472-3481.
(3) Han, G.; Zhang, S.; Boix, P. P.; Wong, L. H.; Sun, L.; Lien, S.-Y. Towards High Efficiency Thin Film Solar Cells. *Prog. Mater. Sci.* **2017,** *87*, 246-291.
(4) Best Research-Cell Efficiencies. Released by National Renewable Energy Laboratory **2016**.
(5) Boix, P. P.; Agarwala, S.; Koh, T. M.; Mathews, N.; Mhaisalkar, S. G. Perovskite Solar Cells: Beyond Methylammonium Lead Iodide. *J. Phys. Chem. Lett.* **2015,** *6*, 898-907.
(6) Jeon, N. J.; Noh, J. H.; Yang, W. S.; Kim, Y. C.; Ryu, S.; Seo, J.; Seok, S. I. Compositional Engineering of Perovskite Materials for High-performance Solar Cells. *Nature* **2015,** *517*, 476-480.
(7) Saliba, M.; Matsui, T.; Seo, J.-Y.; Domanski, K.; Correa-Baena, J.-P.; Nazeeruddin, M. K.; Zakeeruddin, S. M.; Tress, W.; Abate, A.; Hagfeldt, A.; Gratzel, M. Cesium-containing Triple

Cation Perovskite Solar Cells: Improved Stability, Reproducibility and High Efficiency. *Energy Environ. Sci.* **2016,** *9*, 1989-1997.
(8) Saliba, M.; Matsui, T.; Domanski, K.; Seo, J.-Y.; Ummadisingu, A.; Zakeeruddin, S. M.; Correa-Baena, J.-P.; Tress, W. R.; Abate, A.; Hagfeldt, A.; Grätzel, M. Incorporation of Rubidium Cations into Perovskite Solar Cells Improves Photovoltaic Performance. *Science* **2016,** *354*, 206-209.
(9) Ahn, N.; Son, D.-Y.; Jang, I.-H.; Kang, S. M.; Choi, M.; Park, N.-G. Highly Reproducible Perovskite Solar Cells with Average Efficiency of 18.3% and Best Efficiency of 19.7% Fabricated via Lewis Base Adduct of Lead(II) Iodide. *J. Am. Chem. Soc.* **2015,** *137*, 8696-8699.
(10) Correa-Baena, J.-P.; Anaya, M.; Lozano, G.; Tress, W.; Domanski, K.; Saliba, M.; Matsui, T.; Jacobsson, T. J.; Calvo, M. E.; Abate, A.; Grätzel, M.; Míguez, H.; Hagfeldt, A. Unbroken Perovskite: Interplay of Morphology, Electro-optical Properties, and Ionic Movement. *Adv. Mater.* **2016,** *28*, 5031-5037.
(11) Li, X.; Bi, D.; Yi, C.; Décoppet, J.-D.; Luo, J.; Zakeeruddin, S. M.; Hagfeldt, A.; Grätzel, M. A Vacuum Flash–assisted Solution Process for High-efficiency Large-area Perovskite Solar Cells. *Science* **2016,** *353*, 58-62.
(12) Shi, D.; Adinolfi, V.; Comin, R.; Yuan, M.; Alarousu, E.; Buin, A.; Chen, Y.; Hoogland, S.; Rothenberger, A.; Katsiev, K.; Losovyj, Y.; Zhang, X.; Dowben, P. A.; Mohammed, O. F.; Sargent, E. H.; Bakr, O. M. Low Trap-state Density and Long Carrier Diffusion in Organolead Trihalide Perovskite Single Crystals. *Science* **2015,** *347*, 519-522.
(13) Xiao, Z.; Dong, Q.; Bi, C.; Shao, Y.; Yuan, Y.; Huang, J. Solvent Annealing of Perovskite-induced Crystal Growth for Photovoltaic-device Efficiency Enhancement. *Adv. Mater.* **2014,** *26*, 6503-6509.
(14) Noel, N. K.; Abate, A.; Stranks, S. D.; Parrott, E. S.; Burlakov, V. M.; Goriely, A.; Snaith, H. J. Enhanced Photoluminescence and Solar Cell Performance via Lewis Base Passivation of Organic–Inorganic Lead Halide Perovskites. *ACS Nano.* **2014,** *8*, 9815-9821.
(15) Motta, C.; El-Mellouhi, F.; Sanvito, S. Charge Carrier Mobility in Hybrid Halide Perovskites. *Sci. Rep.* **2015,** *5*, 12746.
(16) Sun, C.; Guo, Y.; Duan, H.; Chen, Y.; Guo, Y.; Li, H.; Liu, H. Solvent-assisted Growth of Organic–inorganic Hybrid Perovskites with Enhanced Photovoltaic Performances. *Sol. Energ. Mat. Sol. Cells.* **2015,** *143*, 360-368.
(17) Nie, W.; Tsai, H.; Asadpour, R.; Blancon, J.-C.; Neukirch, A. J.; Gupta, G.; Crochet, J. J.; Chhowalla, M.; Tretiak, S.; Alam, M. A.; Wang, H.-L.; Mohite, A. D. High-efficiency Solution-processed Perovskite Solar Cells with Millimeter-scale Grains. *Science* **2015,** *347*, 522-525.
(18) Yang, M.; Zhang, T.; Schulz, P.; Li, Z.; Li, G.; Kim, D. H.; Guo, N.; Berry, J. J.; Zhu, K.; Zhao, Y. Facile Fabrication of Large-grain $CH_3NH_3PbI_{3-x}Br_x$ Films for High-efficiency Solar Cells via CH_3NH_3Br-selective Ostwald Ripening. *Nat. Commun.* **2016,** *7*, 12305.
(19) Wu, B.; Nguyen, H. T.; Ku, Z.; Han, G.; Giovanni, D.; Mathews, N.; Fan, H. J.; Sum, T. C. Discerning the Surface and Bulk Recombination Kinetics of Organic–Inorganic Halide Perovskite Single Crystals. *Adv. Energy Mater.* **2016**, 1600551.
(20) Zarazua, I.; Han, G.; Boix, P. P.; Mhaisalkar, S.; Fabregat-Santiago, F.; Mora-Seró, I.; Bisquert, J.; Garcia-Belmonte, G. Surface Recombination and Collection Efficiency in Perovskite Solar Cells from Impedance Analysis. *J. Phys. Chem. Lett.* **2016,** *7*, 5105-5113.
(21) Song, Z.; Watthage, S. C.; Phillips, A. B.; Tompkins, B. L.; Ellingson, R. J.; Heben, M. J. Impact of Processing Temperature and Composition on the Formation of Methylammonium Lead Iodide Perovskites. *Chem. Mater.* **2015,** *27*, 4612-4619.

(22) Han, Q.; Bae, S.-H.; Sun, P.; Hsieh, Y.-T.; Yang, Y.; Rim, Y. S.; Zhao, H.; Chen, Q.; Shi, W.; Li, G.; Yang, Y. Single Crystal Formamidinium Lead Iodide (FAPbI3): Insight into the Structural, Optical, and Electrical Properties. *Adv. Mater.* **2016,** *28*, 2253-2258.
(23) Lim, S. S.; Chong, W. K.; Solanki, A.; Dewi, H. A.; Mhaisalkar, S.; Mathews, N.; Sum, T. C. Modulating Carrier Dynamics through Perovskite Film Engineering. *Phys. Chem. Chem. Phys.* **2016,** *18*, 27119-27123.
(24) Correa Baena, J. P.; Steier, L.; Tress, W.; Saliba, M.; Neutzner, S.; Matsui, T.; Giordano, F.; Jacobsson, T. J.; Srimath Kandada, A. R.; Zakeeruddin, S. M.; Petrozza, A.; Abate, A.; Nazeeruddin, M. K.; Gratzel, M.; Hagfeldt, A. Highly Efficient Planar Perovskite Solar Cells through Band Alignment Engineering. *Energy Environ. Sci.* **2015,** *8*, 2928-2934.
(25) Gao, P.; Gratzel, M.; Nazeeruddin, M. K. Organohalide Lead Perovskites for Photovoltaic Applications. *Energy Environ. Sci.* **2014,** *7*, 2448-2463.
(26) Hanusch, F. C.; Wiesenmayer, E.; Mankel, E.; Binek, A.; Angloher, P.; Fraunhofer, C.; Giesbrecht, N.; Feckl, J. M.; Jaegermann, W.; Johrendt, D.; Bein, T.; Docampo, P. Efficient Planar Heterojunction Perovskite Solar Cells Based on Formamidinium Lead Bromide. *J. Phys. Chem. Lett.* **2014,** *5*, 2791-2795.
(27) Xing, G.; Mathews, N.; Lim, S. S.; Yantara, N.; Liu, X.; Sabba, D.; Gratzel, M.; Mhaisalkar, S.; Sum, T. C. Low-temperature Solution-processed Wavelength-tunable Perovskites for Lasing. *Nat. Mater.* **2014,** *13*, 476-80.
(28) Yin, W. J.; Shi, T.; Yan, Y. Unique Properties of Halide Perovskites as Possible Origins of the Superior Solar Cell Performance. *Adv. Mater.* **2014,** *26*, 4653-4658.
(29) Yun, J. S.; Ho-Baillie, A.; Huang, S.; Woo, S. H.; Heo, Y.; Seidel, J.; Huang, F.; Cheng, Y.-B.; Green, M. A. Benefit of Grain Boundaries in Organic–Inorganic Halide Planar Perovskite Solar Cells. *J. Phys. Chem. Lett.* **2015,** *6*, 875-880.
(30) Yang, W.; Yao, Y.; Wu, C.-Q. Origin of the High Open Circuit Voltage in Planar Heterojunction Perovskite Solar Cells: Role of the Reduced Bimolecular Recombination. *J. Appl. Phys.* **2015,** *117*, 095502.
(31) Ryu, S.; Noh, J. H.; Jeon, N. J.; Chan Kim, Y.; Yang, W. S.; Seo, J.; Seok, S. I. Voltage Output of Efficient Perovskite Solar Cells with High Open-circuit Voltage and Fill Factor. *Energy Environ. Sci.* **2014,** *7*, 2614.
(32) Gouda, L.; Gottesman, R.; Ginsburg, A.; Keller, D. A.; Haltzi, E.; Hu, J.; Tirosh, S.; Anderson, A. Y.; Zaban, A.; Boix, P. P. Open Circuit Potential Build-Up in Perovskite Solar Cells from Dark Conditions to 1 Sun. *J. Phys. Chem. Lett.* **2015**, *6*, 4640-4645.

Supporting Information

A facile method to reduce trap density in perovskite photovoltaics

Guifang Han[†], Teck Ming Koh[†], Swee Sien Lim[‡], Teck Wee Goh[‡], Xintong Guo[§,∥], Shin Woei Leow[∥†], Raihana Begum[†], Tze Chien Sum[‡], Nripan Mathews[†∥], Subodh Mhaisalkar[†∥*]*

- **Materials and methods**

Device fabrication

Fluorine doped tin oxide (FTO) substrate was etched using Zn powder and 2M hydrochloric acid (HCl) and subsequently cleaned with Decon soap solution, deionized Water and ethanol. A thin compact layer of TiO_2 was deposited by spray-pyrolysis at 450°C using a solution of titanium diisopropoxide bis(acetylacetonate) (75 wt% in isopropanol) and absolute ethanol (ratio 1:9 by volume). A mesoporous TiO_2 film was deposited by spin-coating TiO_2 paste (30 NR-D, Dyesol) diluted with ethanol (1:5.5 w/w) on the substrate and calcined at 500°C for 30 min. Then 0.1M bis(trifluoro-methane)sulfonimide lithium salt (Li-TFSI) in acetonitrile was spin coated to dope mesoporous TiO_2 according to the report by F. Giordano et al.[1] The doped substrates were annealed at 450°C for 30 min and then transferred into N_2 filled glove box immediately when it cooled down to 150°C.

The triple cation perovskite, $(FA_{0.83}MA_{0.17})_{0.95}Cs_{0.05}Pb(I_{0.83}Br_{0.17})_3$ layer was deposited by single step method as reported in literature. [2] FAI and MABr are purchased from Dyesol. PbI_2 is from TCI, $PbBr_2$ and CsI are from Sigma Aldrich. A mixed solution of FAI (1M), PbI_2 (1.1M), MABr (0.2M) and $PbBr_2$ (0.2M) were dissolved in dimethylformamide: dimethyl sulfoxide 4:1(v:v) with excess PbI_2. 1.5 M CsI stored solution was added into the mixed solution forming the composition required. The triple cation solution was spin-coated on the substrate with a two steps program at 1000 rpm and 6000 rpm for 10 s and 30 s respectively. During the second step, 100 µL chlorobenzene was dropped on the spinning substrate after 15 s. The substrate was then annealed at 100 °C for 60 min. Different concentration (5 ~50 mM) of MABr solution in 2-propanol was spun coated on top of annealed perovskite films at 5000 rpm for 20 s. The film was annealed again at 70 °C for 5 min.

Spiro-OMeTAD solution (70 mg/mL in chlorobenzene) was spin coated on the perovskite spin-coated substrate. Lithium bis(trifluoromethylsulfonyl) imide, tert-butylpyridine and cobalt dopant were added to the above solution. Gold counter electrode was deposited using thermal evaporation method.

Characterization

For the photovoltaic measurements, all devices (0.2 cm^2 active area) were measured by using San-EI Electric, XEC-301S solar simulator (San-EI Electric, XEC-301S) under AM 1.5G standard with a 0.09 cm^2 black mask. Current-voltage (*J-V*) characteristics were recorded using with a Keithley (model 2612A) digital source meter. The crystallographic information of the films were analyzed by Bruker AXS (D8 ADVANCE) X-Ray diffractometer with Cu Kα radiation and a step of 0.02°. The X-Ray diffraction patterns were documented from films deposited on top of FTO coated with

planar TiO_2 film substrates to mimic the solar cell deposition condition. The topographical and cross sectional images were recorded by Field Emission Scanning Electron Microscopy (FESEM, JEOL, JSM 7600F). Absorption spectra of perovskite films were collected by UV-Vis with a Shimadzu UV3600 spectrophotometer.

Surface composition

Surface composition and valance band maximum level are measured by X-ray Photoelectron spectroscopy (XPS) and ultraviolet photoelectron spectroscopy (UPS) respectively. XPS measurements were performed using Omicron EA-125 hemispherical electron analyzer under UHV conditions ($<1\times10^{-9}$ torr). An air-tight sample container was used to transfer the samples from glove box to the load-lock chamber. A monochromatic Al-Kα source with $h\nu$ =1486.6 eV, 200 W was used for XPS measurements. CAE mode was used in both XPS measurements. The pass energy for XPS was 50 eV for wide scans and 20 eV for elemental scans. Elemental analysis was done by fitting Gaussian-Lorentzian profile over Shirley background in each elemental scan.

Photoluminescence, photoluminescence quantum yield and trap density

We performed power dependent steady-state photoluminescence in the low fluence regime (where there is negligible Auger recombination) to estimate the trap densities using a model developed in an earlier work.[3] Briefly, the model assumes an infinite number of trapping pathways, each with their distinct trapping rates and trap densities.

Steady-state photoluminescence of the samples excited with 600 nm pulses were collected using a backscattering geometry at an angle of ~150° by a collimating lens pair. A Coherent OPerA Solo

optical parametric amplifier pumped with a Coherent Libra™ regenerative amplifier (50 fs, 1KHz, 800 nm) was used for the excitation wavelength. The steady-state photoluminescence was collected using a fiber coupled to an Acton Spectra Pro 2500i spectrometer with a Princeton Instruments PIXIS 400B CCD camera.

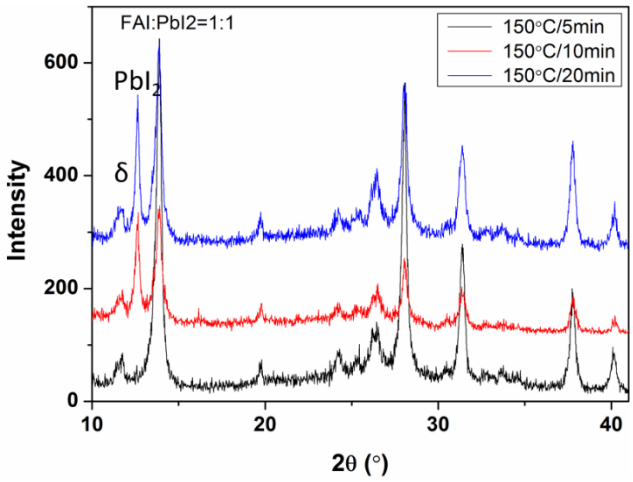

Figure S1 XRD spectrum of $FAPbI_3$ films annealed at 150°C for different dwelling time with FAI and PbI_2 molar ratio of 1:1

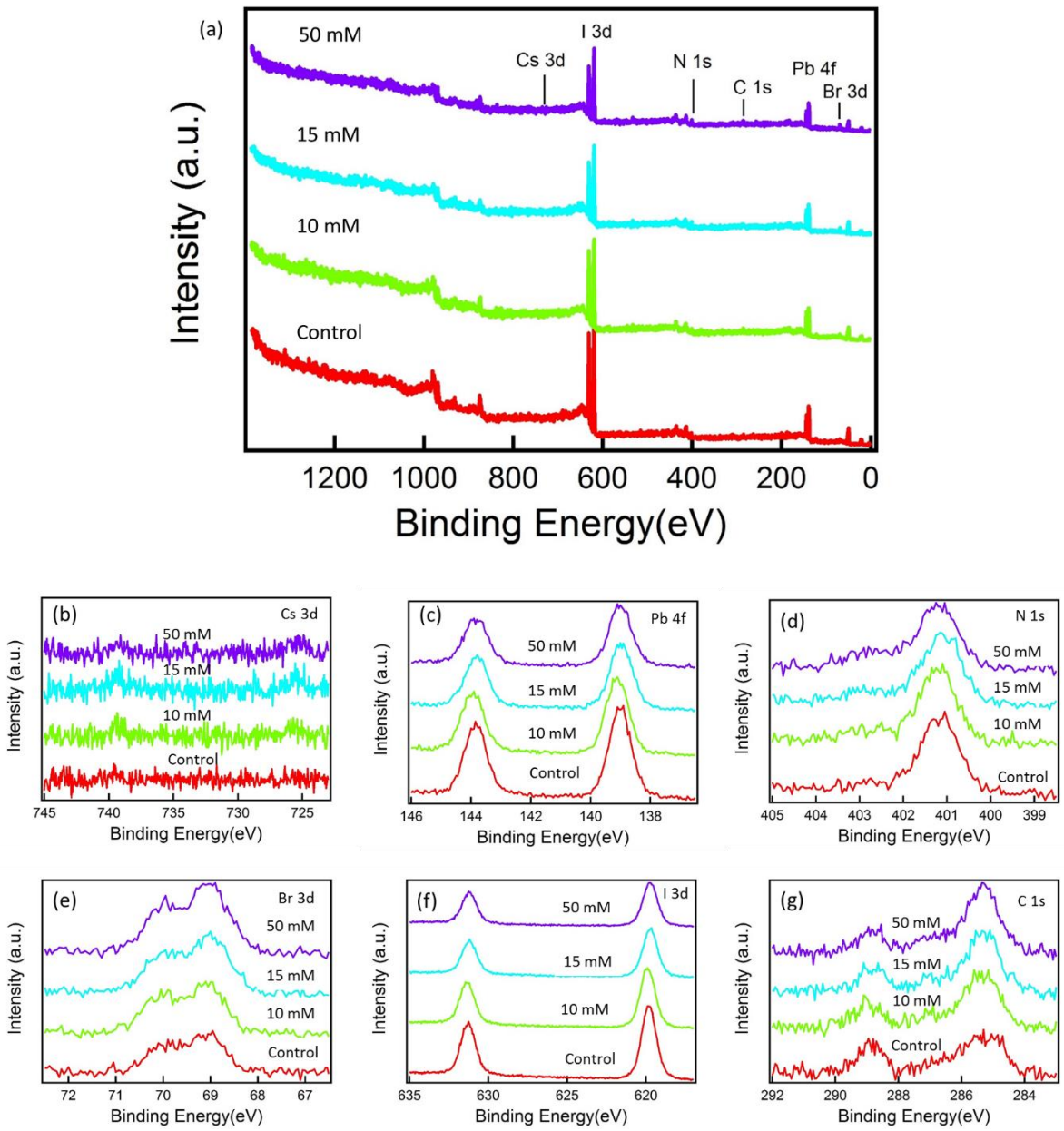

Figure S2 XPS spectrum of the surface of controlled and MABr treated perovskite film, (a) whole spectrum, (b) Cs 3d, (c) Pb 4f, (d) N 1s, (e) Br 3d, (f) I 3d, and (g) C 1s spectrum

- **REFERENCES**

(1) Giordano, F.; Abate, A.; Correa Baena, J. P.; Saliba, M.; Matsui, T.; Im, S. H.; Zakeeruddin, S. M.; Nazeeruddin, M. K.; Hagfeldt, A.; Graetzel, M., Enhanced Electronic Properties in Mesoporous TiO_2 via Lithium Doping for High-efficiency Perovskite Solar Cells. *Nat. Commun.* **2016**, *7*, 10379.

(2) Saliba, M.; Matsui, T.; Seo, J.-Y.; Domanski, K.; Correa-Baena, J.-P.; Mohammad K, N.; Zakeeruddin, S. M.; Tress, W.; Abate, A.; Hagfeldt, A.; Gratzel, M., Cesium-containing Triple Cation Perovskite Solar Cells: Improved Stability, Reproducibility and High Efficiency. *Energy Environ. Sci.* **2016**, *9*, 1989-1997.

(3) Xing, G.; Mathews, N.; Lim, S. S.; Yantara, N.; Liu, X.; Sabba, D.; Gratzel, M.; Mhaisalkar, S.; Sum, T. C., Low-temperature Solution-processed Wavelength-tunable Perovskites for Lasing. *Nat. Mater.* **2014**, *13*, 476-80.